Effects of inclusions on the performance of a solid rocket motor

Effects of Inclusions on the Performance of a Solid Rocket Motor

F. Ponti[1], S. Mini[2], L. Fadigati[3] and V. Ravaglioli[4]
University of Bologna, Forlì, FC, 47121, Italy
A. Annovazzi[5], V. Garreffa[6]
Avio Space Propulsion, Colleferro, Rome, 00034, Italy

Abstract

Some of the most common defects that can be generated during the production of solid propellant are voids and porosity, usually associated with the casting process, and cracks and debonding, typically initiated by the high stresses caused by the curing process. This paper presents the development of an algorithm capable of evaluating the burning surface regression of a solid rocket booster when inclusions are present within the grain. The effects produced by the cavities are evaluated both in terms of performance (i.e., comparison with the behavior of the nominal combustion surface), and in terms of safety (i.e., evaluation of the thermal protection increased exposure). The paper also documents the influence of uncertainties in the knowledge of the real dimension and position of the inclusions detected within the motor. The radiography inspection of the motor is able to detect the presence of cavities within a certain level of accuracy, and the worst combination of these uncertainties has to be determined in order to guarantee, even under such circumstances, the safe and successful firing of the motor. The methodology developed in the paper is adapted in order to identify the worst uncertainty combination, and to subsequently determine the corresponding performance deviation.

[1] Full Professor, Department DIN, via Fontanelle 40, fabrizio.ponti@unibo.it

[2] Research Fellow, Department DIN, via Fontanelle 40, stefano.mini3@unibo.it

[3] PhD Candidate, Department DIN, via Fontanelle 40, luca.fadigati2@unibo.it

[4] Senior Assistant Professor, Department DIN, via Fontanelle 40, vittorio.ravaglioli2@unibo.it

[5] Senior Engineer, AVIO Space Propulsion Design Department, adriano.annovazzi@avio.com

[6] Senior Engineer, AVIO Space Propulsion Design Department, valentina.garreffa@avio.com

KEYWORDS: grain inclusions, solid rocket motor flaws, burning surface regression, spherical cavity effect.

1 Introduction

The manufacturing process of a solid rocket motor has to be carefully designed in order to obtain a perfect match between the design specifications and the final geometry, thus ensuring that performance and reliability are aligned with the expectations. Unfortunately, even a perfectly designed process may involve issues that can generate undesired defects and deviations [1] with respect to the expected geometry and properties of the motor [2], [3].

One of the procedures typically susceptible to defects affecting both the performance and reliability of a motor is the casting process [4]. While casting, for example, the propellant may not adhere perfectly to the case: in this instance, a portion of the interface surface between propellant and case may detach during the following manufacturing operations (i.e., vulcanization, handling, etc.). Handling and thermal expansion may even cause the solid propellant to crack, increasing its apparent porosity. Another issue may be the presence of cavities within the grain, due, for example, to the high viscosity of the propellant and to a number of voids forming due to the entrapment of air during the casting phase. The entity of the aforementioned defects could even degenerate once the combustion process is initiated, and their stability has to be verified in relation to the loads generated by internal pressure and rocket acceleration [5].

For these reasons, every time a motor is manufactured, an extensive monitoring campaign is performed in order to check its integrity and the possible presence of the previously mentioned – and other – defects. For example, the motor may be examined using X-ray, magnetic resonance or ultrasound techniques that allow to identify the presence of inclusions or detachments, and to evaluate their extension and localization within the motor [6–8]. Once a single defect or numerous ones are identified, the following task is to quantify the effects generated by its or their presence, both in terms of performance and reliability, and to determine whether the motor may be safely and efficiently launched or not [9,10].

One of the most common defects that are identified during the monitoring campaign is the presence of inclusions within the propellant, resulting from air bubbles, air gaps, and cavities that remain trapped within the high-viscosity propellant during the casting process. The presence of porosities causes two main effects: a faster progression of the combustion process, when each inclusion is reached by the burning surface, and a quicker exposure of the thermal protections, that are reached sooner by the high-temperature gases produced within the combustion chamber. The first effect causes a change in the instantaneous value of the surface exposed to combustion, thus modifying the thrust profile and the performance of the motor, whereas the second one mainly affects the reliability of the motor, since thermal protections are usually designed to

last for a definite period of time while exposed to the hot gases in the combustion chamber, and a longer exposure may completely consume the available layer of thermal protection.

If numerous inclusions are present within the propellant, investigating their effect on the performance of the motor may become even more complex, due to the mutual influence on the progression of the combustion surface. In addition to this, it should be underlined that the presence of defects is detected through measurements that are affected by inaccuracies; consequently, the evaluation of the modification in the performance profile and the reduction in reliability should be carried out so as to take into account the worst possible effects, identified by combining flaws in the most dangerous possible way.

In the past, many approaches were developed in order to determine the 3D evolution of the combustion surface of solid rocket motors; some of them were conceived through the so-called level-set method [11] or by defining a distance function [12–14]. Usually, these types of methodologies are not able to deal with propellant heterogeneities [15–17] and may provide a performance evaluation only under nominal conditions. Some of them have been evolved [18–21] to consider the heterogeneities that may be produced by the casting process [22,23] or by the granulometric composition of the propellant [24–27], whose effect is a local change of the burning speed [28–31]. In other cases, a meshing procedure is used either to represent the 3D grain geometry [32–34] or to discretize the 2D burning surface [35–37]. These approaches may succeed in considering a point-by-point variation of the regression rate, thus simulating the non-isotropic burning of a typical solid propellant [38,39]; some of them, by the same authors of this paper [40] have also proven to be capable to treat inclusions and defects [41]. The expected accuracy of these methodologies is related to the resolution of the meshes generated to describe the 3D or 2D geometries of the grain or of its surface. The attempt to increase mesh resolution results in a very large number of vertices, hence in a large computational effort. If the size of the identified inclusions is small, the need to precisely describe their geometry would subsequently require a really fine mesh, and the number of involved vertices would increase significantly. In the case of a large number of inclusions found in a motor of great size, the problem becomes even harder to be correctly solved, and for this reason the number of inclusions that can be treated with these tools is usually limited to some tenths.

The recent evolution of diagnostic systems made it possible to identify an increasing number of defects of reduced dimensions [42]. On the one hand, this advancement allows to determine the thrust profile of each motor with greater precision, and therefore, to assess more accurately if the calculated performance would fall within the acceptance limits; on the other hand, managing many small-sized defects would make the task of estimating the precise performance profile of the actual manufactured – and imperfect – motor harder to be obtained, on account of two conflicting needs, which are: to obtain a good description both of the defects and of the burning surface of the motor, and to maintain the computational effort at a reasonable level. For a very high number of inclusions the solution with the existing tools becomes unpractical.

In order to evaluate the consequences generated by a large number of small inclusions precisely, it is therefore necessary to develop a dedicated tool which is able to predict both the performance change and reduction in reliability, given estimates of the dimensions and location of the cavities. This paper illustrates a new geometric approach that is capable of reaching such a goal for an unlimited number of small spherical inclusions that are present into the grain, identifying both the ensuing modifications in the performance profile and the increase in the time of exposure of thermal protections to hot gases. The approach is developed using the 3D nominal regression of the burning surface as input, evaluated through a solid rocket motor tool developed by the authors of this paper, namely ROBOOST. The geometric evolution of the combustion surface provided by ROBOOST is used to assign a web coordinate to each position within the grain. Such coordinate identifies the distance covered by the combustion process on its path to reach that position, starting from the initial combustion surface; the developed methodology ultimately allows to assess the web coordinate variations caused by the presence of the investigated inclusions [43].

Another important attribute of the developed algorithm is the capability of assessing the influence of the dimension and position uncertainties of the inclusions on the calculated web difference, focusing on the evaluation of the worst possible combination of the measured uncertainties, both on a global and local scale. The developed approach has been validated using an example in which an analytical solution is known and used to evaluate the effects of a large set of inclusions detected on a real rocket; the algorithm has been finally integrated into ROBOOST in order to increase its capability of simulating solid rocket motors.

The paper is divided into three main sections, organized as follows: the first section presents the developed approach; the second shows the validation of the methodology applied to some test cases whose analytical solution is known; the third section discusses the results obtained by applying the algorithm to a real motor with a large number of identified inclusions.

2 Methodology Description

2.1 Combustion surface nominal regression and web coordinate definition

The first step of the developed methodology is the definition of the web coordinate, w, determined using the nominal regression of the combustion surface. Web coordinate is indeed defined, for each position within the grain, as the distance covered by the combustion process on its path, i.e., the total grain thickness burnt to reach that position. If the propellant has an isotropic behavior, without heterogeneities, the web coordinate value (from now on referred to as “web value”) corresponds to the minimum distance measured from the initial combustion surface. If the burning propellant is not isotropic, however, the web value and the minimum distance may differ, due to the dissimilar regression rates that may be applied in the different directions of the combustion progression. For this reason, the calculation of the web value is performed by

assigning to the points belonging to the combustion surfaces, evaluated at each instant of time, a web equal to the integral of the nominal regression rate with respect to time. If the instantaneous combustion surface has been calculated by taking into account the non-isotropic behavior of the propellant, the web value will be determined accordingly. The described approach is also valid for isotropic propellants, since the integral of the nominal regression rate coincides, in this case, with the minimum distance evaluation. Nevertheless, its application is more general, since it allows to consider even the potential non-isotropic behavior of the propellant; for this reason, it is the preferred one. A tool that is capable of calculating the combustion surface regression also under these conditions has been developed by the same authors of this work and is described in previous papers on the topic [40]. Since the development of that tool (ROBOOST) is well beyond the scope of the present study, the details of its working mechanism are not described in this paper, and its outputs are used, as already mentioned, to obtain the web value. An example of this process is described in the following Figures, in which the surface regression of a finocyl motor is represented in normalized units.

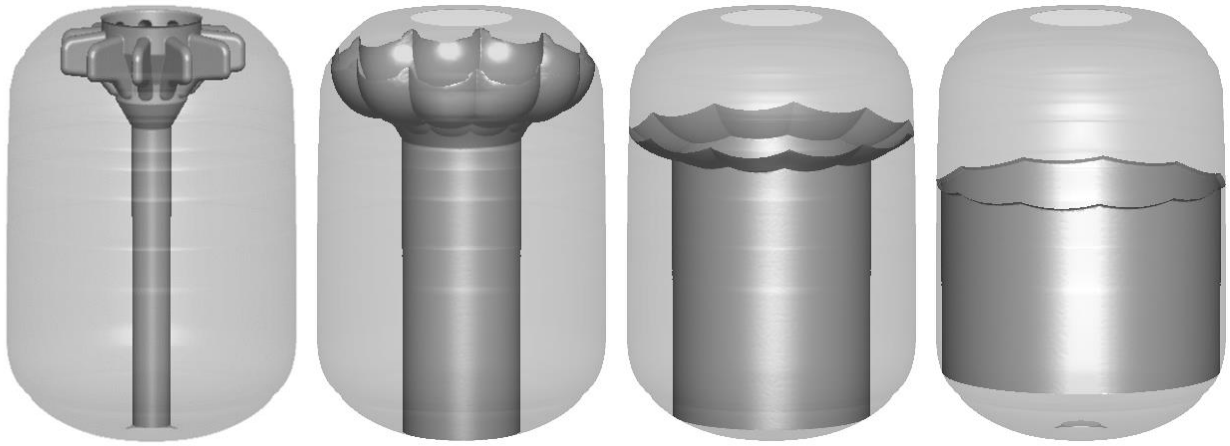

a) Norm. web 0.00 b) Norm. web 0.32 c) Norm. web 0.64 d) Norm. web 0.96

Fig. 1: Combustion surface at different normalized web coordinates in a finocyl motor

Each of the surfaces represented in Fig. 1 is associated to a precise value of the web (expressed in normalized units). The web distance between two consecutive surfaces has been fixed as equal to $5 \cdot 10^{-4}$ normalized web. The availability of such a large number of combustion surfaces at different web coordinates allows for the evaluation of the web coordinate value at each internal position of the motor, as described in Fig. 2, where some characteristic sections are shown.

The web value obtained for each position within the motor can be now represented as a function of the coordinates of that position, as described by the following equation:

$$w = w(x, y, z) \tag{1}$$

2.2 *Evaluation of the path followed to reach the motor case*

The same set of combustion surfaces may also be used to evaluate the path that is followed by the combustion process to reach each of the positions located on the motor case. This can be done by reverse integrating the local normal to the combustion surface, starting from each location on the motor case, until a corresponding position on the initial combustion surface is reached. Some combustion paths, obtained for the same motor geometry considered in the previous figures, are shown as an example in Fig. 3. Knowing the followed path is important for the evaluation of the danger associated to each inclusion, since an inclusion that is located on the path followed by the combustion process to reach a position on the motor case will be more dangerous for that position, with respect to inclusions far from that path.

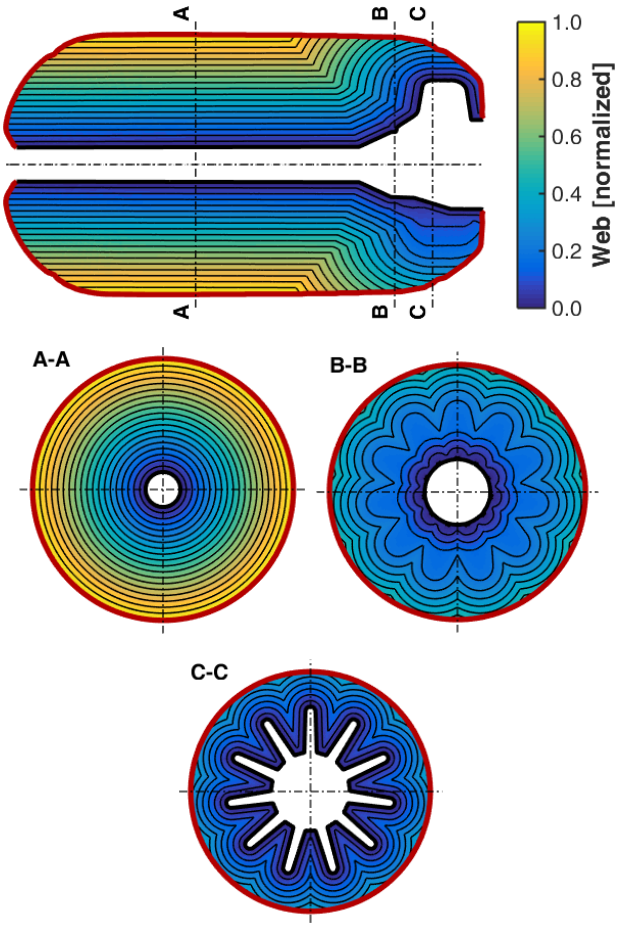

Fig. 2: Web coordinate representation in some characteristic sections of the motor

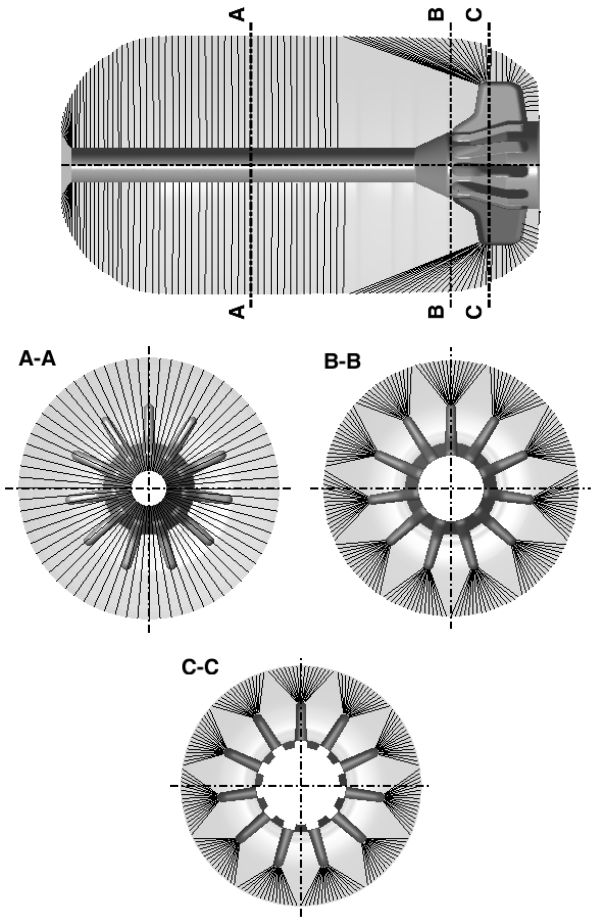

Fig. 3: Combustion paths followed to reach different locations on the motor case

2.3 Effect of a spherical cavity on a grain position

The second step of the methodology is the evaluation of the effects of a single spherical cavity placed in a generic position within the grain. The spherical inclusion is identified by its diameter D_{cav} and by the position of its center (x_{cav}, y_{cav}, z_{cav}); the use of Equation (1) allows to determine the web coordinate w_{cen} in which the center of the cavity would have been reached by a nominal combustion:

$$w_{cen} = w(x_{cav}, y_{cav}, z_{cav}) \tag{2}$$

The cavity is reached by the combustion process at a web value w_{cav} that is lower than w_{cen}, as clearly displayed in Fig. 4 and reported in Equation (3).

$$w_{cav} = w_{cen} - \mathrm{D}_{cav}/2 \tag{3}$$

As soon as the cavity is reached by combustion, its internal surface becomes part of the burning process and the regression begins to proceed, propagating in all directions.

A generic point P of coordinates (x_p, y_p, z_p), under nominal conditions, would have been reached by the combustion process at a web coordinate w_p:

$$w_p = w(x_p, y_p, z_p) \tag{4}$$

Due to the presence of the inclusion, the same point could be reached by the combustion process at a different web coordinate. Following the combustion path that goes through the cavity, it is then possible to determine that the generic point could be reached by the combustion coming from the inclusion at a web coordinate $w_{p\,cav}$, which is equal to:

$$w_{p\,cav} = w_{cav} + dist_{p\,cav} - \mathrm{D}_{cav}/2 \tag{5}$$

where $dist_{p\,cav}$ is the distance between the center of the cavity and point P (see Fig. 4).

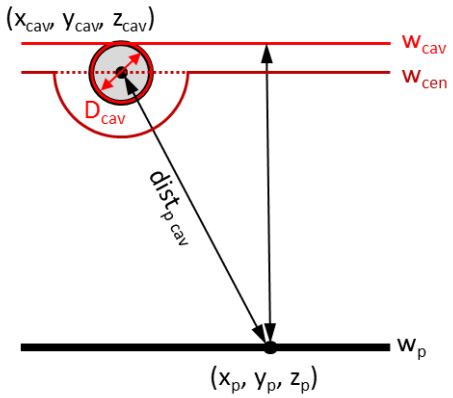

Fig. 4: Graphic representation of the effect of a cavity on a grain position

If $w_{p\,cav} > w_p$, the presence of the cavity does not produce any effect on the combustion timing for the point P. On the other hand, if $w_{p\,cav} < w_p$, the presence of the inclusion causes an advance ($\Delta w_{p\,cav} = w_p - w_{p\,cav}$) of the web value in which point P is reached by combustion, as expressed by Equation (6):

$$\Delta w_{p\,cav} = \begin{cases} 0 & , \text{ if } w_{p\,cav} > w_p \\ w_p - w_{cen} - dist_{p\,cav} + \mathrm{D}_{cav}, & \text{if } w_{p\,cav} < w_p \end{cases} \tag{6}$$

The condition expressed by Equation (6) allows to split the web that is reached by the combustion process after the incorporation of the cavity into two separate regions: the one that is affected by the presence of

the inclusion (characterized by a positive value of the web advance (zone of influence)); the one that is not affected by the cavity.

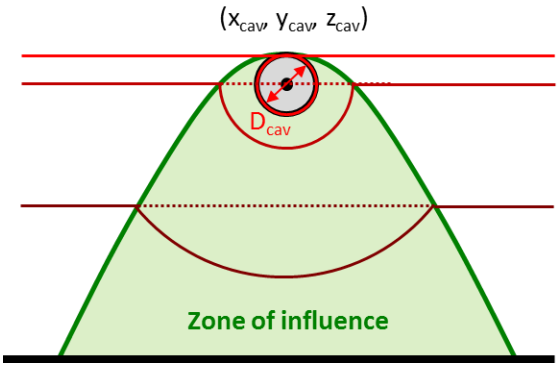

Fig. 5: Zone of influence of a cavity

2.4 Effect of a cavity on another cavity

If more than one cavity is present within the grain, they may exert a mutual influence on each other, and for this reason, the web in which each inclusion is reached by the combustion process may differ from that obtained under nominal conditions. This scenario is schematized in Fig. 6:

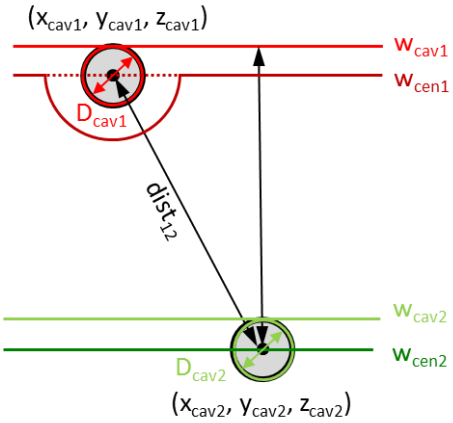

Fig. 6: Graphic representation of the effect of a cavity on another cavity

The second cavity shown in Fig. 6 is reached by the combustion surface under nominal conditions (i.e., without any influence from the first inclusion) at a web coordinate:

$$w_{cav2} = w_{cen2} - \mathrm{D}_{cav2}/2 \tag{7}$$

Due to the presence of the first cavity, the combustion process may reach the second inclusion through a path that crosses the first one, at a web coordinate:

$$w_{cav2\,cav1} = w_{cen1} - \mathrm{D}_{cav1} + dist_{12} - \mathrm{D}_{cav2}/2 \tag{8}$$

The presence of the first cavity determines an advance of the web ($\Delta w_{21} = w_{cav2} - w_{cav2\,cav1}$) in which the second inclusion is reached by combustion only when $w_{cav2\,cav1} < w_{cav2}$, otherwise no mutual influence may be exerted among the considered inclusions, as expressed by Equation (9).

$$\Delta w_{21} = \begin{cases} 0 & , \text{ if } w_{cav2\,cav1} > w_{cav2} \\ w_{cen2} - w_{cen1} - dist_{12} + \mathrm{D}_{cav1}, & \text{if } w_{cav2\,cav1} < w_{cav2} \end{cases} \tag{9}$$

2.5 Effect of two cavities on the position of a grain

The next step is the study of the effects generated by the two inclusions considered in the previous step on a generic point P of coordinates (x_p, y_p, z_p). As can be seen in Fig. 7, point P can be reached by combustion through 3 different paths:

- Nominal combustion reaches point P at web $w_p = w(x_p, y_p, z_p)$
- Combustion surface coming from the first cavity at web $w_p - \Delta w_{p1}$
- Combustion surface coming from the second cavity at web $w_p - \Delta w_{p2}$

each of them causing a web advance, as expressed by Equation (10).

$$\begin{cases} 0 \\ \Delta w_{p1} = w_p - w_{cen1} - dist_{p1} + \mathrm{D}_{cav1} \\ \Delta w_{p2} = w_p - w_{cen2} - dist_{p2} + \mathrm{D}_{cav2} + \Delta w_{21} \end{cases} \tag{10}$$

The shortest path is the only one to be considered to evaluate the web coordinate in which point P is reached by combustion; the web advance for point P (Δw_p) can be therefore determined as the maximum of the web advances associated to each of the possible paths:

$$\Delta w_p = max(0, \Delta w_{p1}, \Delta w_{p2}) \tag{11}$$

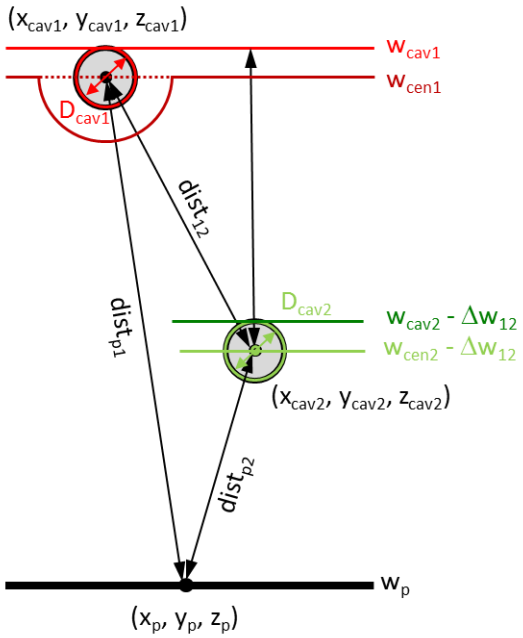

225

226 **Fig. 7: Graphic representation of the effects of two cavities on a generic position of the grain**

227 The approach may now be extended to a generic set of inclusions by simply taking into account that the
228 web advance of a single cavity is determined as the maximum of the mutual influences generated by all the
229 other inclusions, each of them considered with its own web advance, in turn caused by the other cavities.
230 For a generic i-th cavity, out of a set of N cavities, the web advance Δw_i can be measured as:

231 $$\Delta w_i = max(0, \Delta w_{i1}, \dots, \Delta w_{iN}) \quad (12)$$

232 Even if the process seems complex due to the apparent large number of mutual influences to be taken into
233 account, it can be strongly simplified by considering a tree of influences between cavities built bearing in
234 mind that if cavity 1 influences cavity 2, it can be stated that cavity 2 does not influence cavity 1. Such tree
235 can be built simply by looking at the web in which each of the cavities should be reached by combustion
236 under nominal conditions, referred to as $w_{cav\,i}$, and then by sorting them using this quantity. The influence
237 on a specified cavity i by another cavity j is studied only when $w_{cav\,i} > w_{cav\,j} - w_{tol}$, where w_{tol} is a tolerance
238 value that guarantees that the influencing cavities are considered even when the initial order is changed by
239 the application of the relative influence.
240 Once the web advance Δw_i has been measured for each inclusion, the effect of the N inclusions on a generic
241 point P within the grain can be obtained as the largest value among the web advances generated by each
242 cavity on that point:

$$\Delta w_p = max\left(0, \Delta w_{p1}, \dots, \Delta w_{pN}\right) \quad (13)$$

If point P is located within the grain, the methodology presented above allows to evaluate the burning surface change that is caused by a given set of inclusions and, consequently, also the performance variation of the SRM under study. If point P is located on the thermal protection, the evaluation of the web advance allows to estimate the increase of exposure to the hot gases generated by combustion that the set of cavities is causing on that point of the thermal protection.

The methodology described in this paper is based on a scenario involving spherical cavities because they are the most common type of inclusions that can be observed and detected in a solid rocket motor. However, such approach can be extended also to cavities with a generic shape simply by considering their shape as obtained from a combination of elementary inclusions shaped like spheres. Such a process may always be set up to describe generic shapes, the only side effect being the increased number of cavities to be considered.

2.6 Effect of uncertainties

The effects discussed in the previous sections are computed using the nominal diameter and positioning of the cavities. Each cavity is known through experimental observations of the manufactured motor, and nominal diameter and position are affected by uncertainties that can produce different evaluations of the web advance. The goal is to evaluate the worst-case scenario by taking into account all the uncertainties.

In order to perform this operation, the effect of a single cavity on the web advance of a generic point is studied, as obtained through Equation (6):

- The larger the diameter of the cavity, the larger the effect on the exposure map (since it implies a larger value of D_{cav} in Equation (6));
- The effect generated by a cavity on the point under study is most substantial when the cavity is located along the path followed by the regression surface to reach that point (this implies a lower value of $w_{cen}+dist_{p\ cav}$, that appears with a negative sign in Equation (6)).

The same considerations may be extended also to a combination of two (or more) cavities:

- The larger the diameter of each cavity, the most pronounced the combined effect;
- The more the cavities are aligned along the path followed by the regression of the surface, the most pronounced the effect on the point under study.

Figure 8 describes the concept of cavity alignment, highlighting that for each position within the grain, the worst condition for that position would be obtained by applying the uncertainties with different combinations.

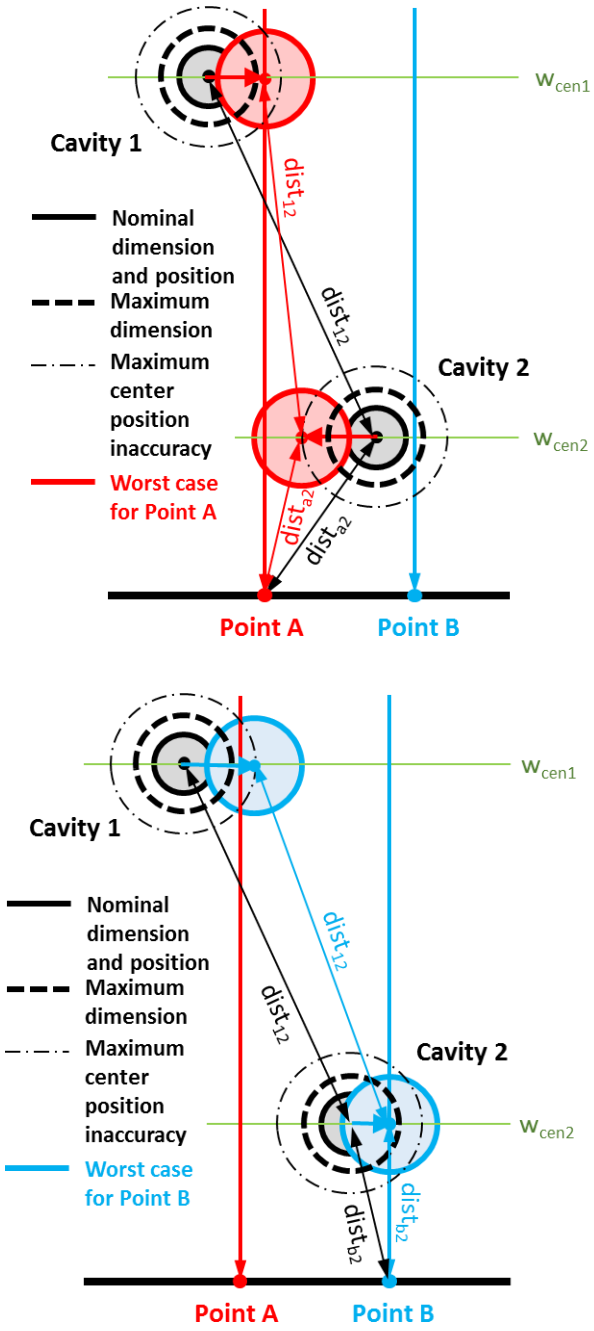

Fig. 8: Graphic representation of the worst-case inaccuracy application for two different points A and B

Based on these considerations, it can be stated that the absolute worst combination of inaccuracies does not exist, since the worst-case configuration may differ for each point. If these considerations are applied to the motor case, this means that the worst possible web advance should be evaluated independently for each position on the case. By combining the worst-case conditions for each point on a surface (e.g., the thermal

protection surface), it is possible to obtain a map that can be referred to as the worst-case map for that surface.

3 Methodology Validation

3.1 Comparison with test cases

The developed methodology has been used to determine the variations of the burning surface due to the presence of cavities for three test cases, whose results can be determined through simple geometric considerations. The three cases have been designed to investigate different types of interaction between the burning surface and the inclusions, also considering different mutual influences that may be exerted among cavities. In all test cases, a planar combustion surface has been considered to guarantee a precise evaluation of the ideal surface variation; the planar surface incorporates one or more inclusions in the following way:

A. A single inclusion;
B. A sequence of two inclusions placed along the same combustion progression line;
C. Two identical inclusions located at the same web coordinate.

For each test, the nominal combustion surface has been discretized using a triangular mesh, and the effects of the cavities have been evaluated by applying the described methodology to each vertex of the mesh. The extension of the nominal and the modified surface has been determined by summing up all the areas of the mesh triangles. Finally, the difference between nominal and modified areas has been compared with the same difference obtained through geometric computations.

3.1.1 Test A

A single inclusion with a diameter D_{cav}=16 mm and center (x_{cav}, y_{cav}, z_{cav}) = (0, 100, 0) mm is incorporated by a planar combustion surface characterized by a regression direction aligned with the y-axis. When the surface reaches a position in the y direction equal to 140 mm, the effect of the cavity appears as a spherical cap, with radius R equal to 56 mm and cap height h equal to the inclusion diameter of 16 mm. The surface of the spherical cap can be measured as $2\pi Rh$, whereas the surface of the plane that is substituted by the spherical cap is equal to $\pi(R^2-(R-D_{cav})^2)$. The surface increase due to the cavity is therefore the difference of these surfaces, equal to πh^2=804.25 mm^2.

Figure 9a reports the result of the methodology described in the previous section applied to a triangular mesh with a maximum edge size equal to 0.4 mm. The estimation of the surface increase is 799.50 mm^2, with a percent error of 0.59%.

3.1.2 Test B

Two inclusions with diameters D_{cav1}=16 mm and D_{cav2}=8 mm and centers (x_{cav1}, y_{cav1}, z_{cav1}) = (0, 100, 0) mm and (x_{cav2}, y_{cav2}, z_{cav2}) = (0, 130, 0) mm are incorporated by a planar combustion surface, in a similar way to what was described in Test A. When the surface reaches a position in the y direction equal to 140 mm, the effect of the cavities appears as a combination of two spherical caps, with radiuses R equal to 56 mm and 34 mm respectively, and cap heights h equal to 16 mm and 24 mm respectively. The intersection between the two spherical caps is observed at a height equal to 8 mm, meaning that the first 8 mm of the combined surface are obtained as a portion of the first spherical cap (that becomes a spherical sector of height h_1), while the following 16 mm are the final portion of the second spherical cap of height h_2 (see Fig. 9b for more details).

The extension of the described surface can be therefore evaluated as the sum of the area of a spherical sector and a spherical cap, obtaining $2\pi R_1 h_1 + 2\pi R_2 h_2$, whereas the surface of the plane that is substituted by the spherical cap is equal to $\pi(R_1^2 - (R_1 - D_{cav1})^2)$. The surface increase due to the cavity is therefore equal to the difference of these surfaces, amounting to 1407.44 mm^2.

Figure 9b reports the result of the methodology developed in this paper applied to a triangular mesh with a maximum edge size equal to 0.4 mm. The estimation of the surface increase is 1401.20 mm^2, with a percent error of 0.44%.

3.1.3 Test C

Two inclusions, both with diameters of 20 mm and centers (x_{cav1}, y_{cav1}, z_{cav1}) = (0, 140, 16) mm and (x_{cav2}, y_{cav2}, z_{cav2}) = (0, 140, -16) mm respectively are incorporated by a planar combustion surface in a similar way to Test A. When the surface reaches a position, in the y direction, equal to 140 mm, the effect of the cavities appears as a combination of two portions of spherical cap, with radiuses R equal to 20 mm, cap heights h equal to 20 mm, with a missing portion of cap whose height is h_m= 4 mm (see Fig. 9c for more details).

The extension of the described surface can be evaluated as the sum of two semispherical caps (thus obtaining a spherical cap), whereas the surface of the plane that is substituted can be obtained as the sum of two circular segments. The surface increase due to the cavity is the difference of these surfaces, which is equal to 2141.42 mm^2.

Figure 9c reports the result of the methodology developed in this paper, applied to a triangular mesh with maximum edge size equal to 0.4 mm. The estimation of the surface increase is 2133.70 mm^2, with a percent error of 0.39%.

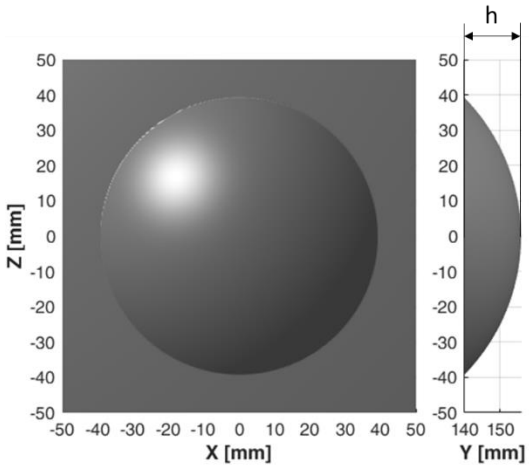

Test A

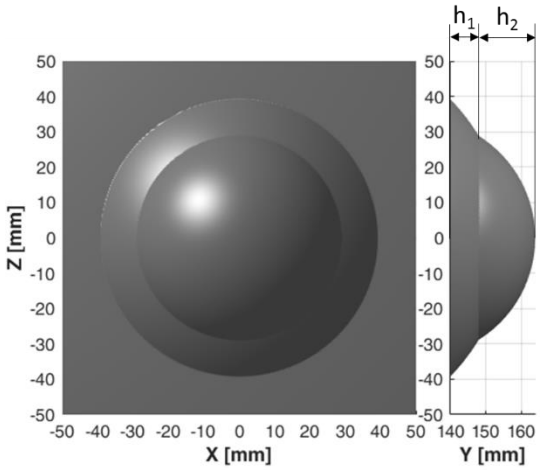

Test B

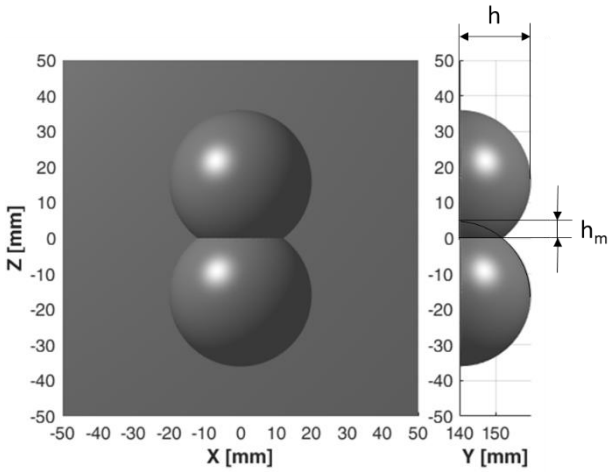

Test C

Fig. 9: Results obtained in three different test cases

The obtained error for the test cases taken into account is satisfactory and allows to state that the validation of the methodology has been successful. Nevertheless, accuracy depends on the chosen resolution to generate the mesh used to describe the surfaces. An investigation of the effects of the resolution has been carried out obtaining the results shown in Fig. 10. As can be observed, in order to obtain an accurate evaluation of the effects generated by the cavities taken into account, the maximum edge size should be lower than $1\ mm$. Since the diameter of the inclusions ranges from 8 to $20\ mm$, it can be stated, as a general rule, that the dimension of the edge size of the mesh should be smaller than $1/10$ of the diameter of the cavities under investigation.

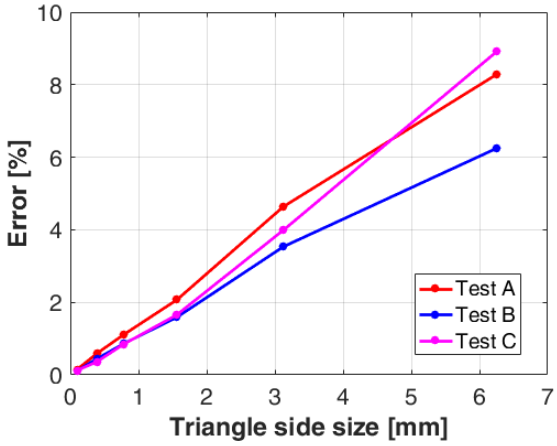

Fig. 10: Percent error variation as a function of the mesh edge size

4 Results and discussion

The developed methodology has been used to investigate the effects generated by a large number of cavities found on an actual motor. A significant number of cavities (670) had been generated during the casting process of a segment of the Ariane 5 solid rocket motor namely segment S3. The presence of the cavities has been detected through the diagnostic procedures that follow the manufacturing phase, by employing an X-ray instrumentation.

Since the detected cavities are localized in a relatively small portion of the motor, the investigation of their effects was focused on that portion, thus neglecting a large part of the original geometry, and considering only the interesting one. The geometry of the part considered in for the present study is represented in Fig. 11, together with the location of the detected cavities. Neglecting the portion of the motor with no detected

inclusions is useful to reduce the computational effort needed (the higher the extension of the motor, the larger the number of triangles to be used to cover the entire combustion surface), and/or increase the accuracy of the evaluations.

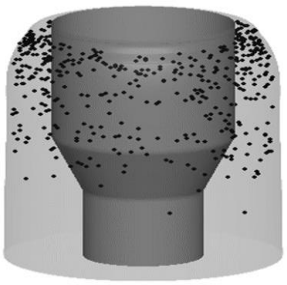

Fig. 11: Geometry of the investigated portion of the motor with the detected cavities

The portion of the motor has been studied in its nominal configuration to identify the web coordinate and the path followed by combustion to reach the motor case, so as to develop the methodology used to evaluate the effects of the cavities precisely. The process that allows to determine this piece of information requires the knowledge of the combustion surface regression at different web values, obtained through the tool introduced at the beginning of this work (ROBOOST) and displayed in Fig. 12:

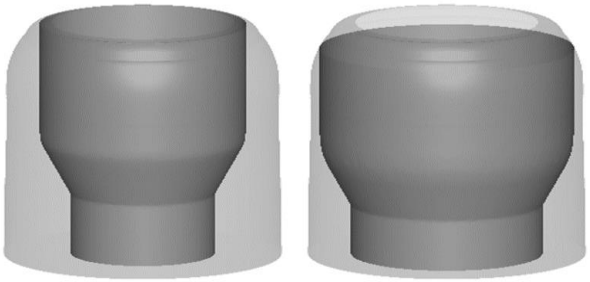

a) Norm. web 0.15 b) Norm. web 0.45

c) Norm. web 0.75

Fig. 12: Regression of the combustion surface at different web values

The extension of the combustion surfaces measured at different web coordinates by ROBOOST has been displayed in Fig. 13 as a function of the web coordinate, represented in a normalized form for confidentiality reasons. Since the surface is evaluated on a portion of the entire motor, its waveform does not represent the complete generated thrust directly, even if the difference caused by the inclusions is the same as the one that affects the whole motor.

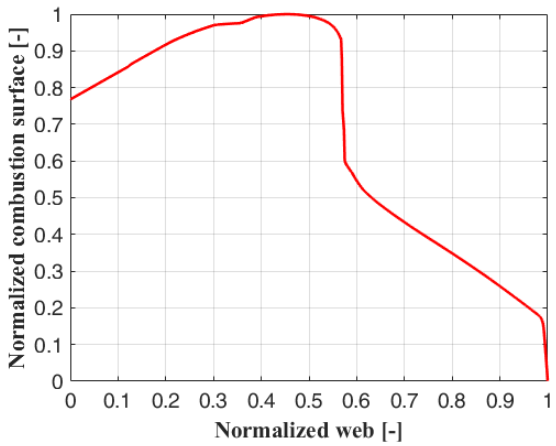

Fig. 13: Combustion surface vs web coordinate

The knowledge of the combustion surfaces reported in Fig. 12 allows to determine the web coordinate value, shown in Fig. 14, following the same procedure already described in a previous section of this paper. As for Fig. 15, it illustrates the lines describing the path followed by the combustion process to reach each of the available positions on the motor case.

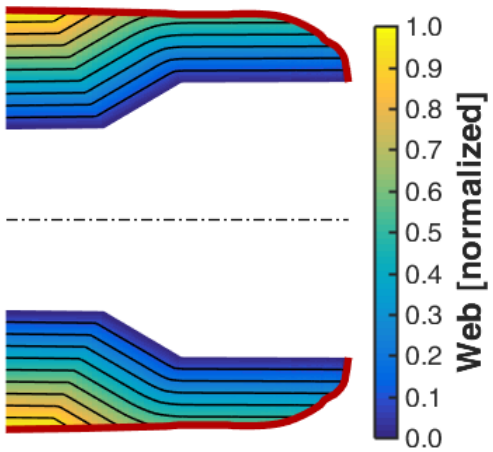

Fig. 14: Web coordinate representation for the longitudinal section of the motor

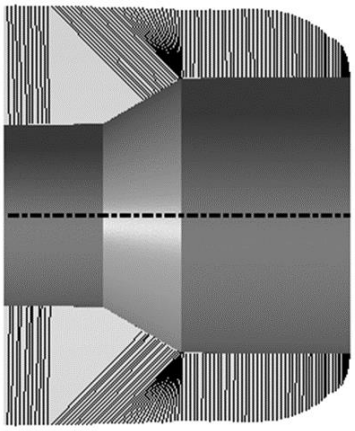

Fig. 15: Combustion paths followed to reach the different locations on the motor case

As already mentioned, 670 cavities with a diameter ranging from 5 to 14 *mm* have been detected on this motor; consequently, a very fine mesh was required to describe the surface regression. The location of each cavity has been used to evaluate the web coordinate of the centers, and to sort them based on the expected order of incorporation into the combustion surface (i.e., based on the web coordinate). This piece of information is very useful to determine the mutual influence of the various inclusions efficiently, as already explained in a previous section. Fig. 16 illustrates the number and total volume of the cavities as a function of the web coordinate, showing that the largest part of the inclusions is contained in the first half of the web coordinate (i.e., approximately in the first half of the duration of the combustion).

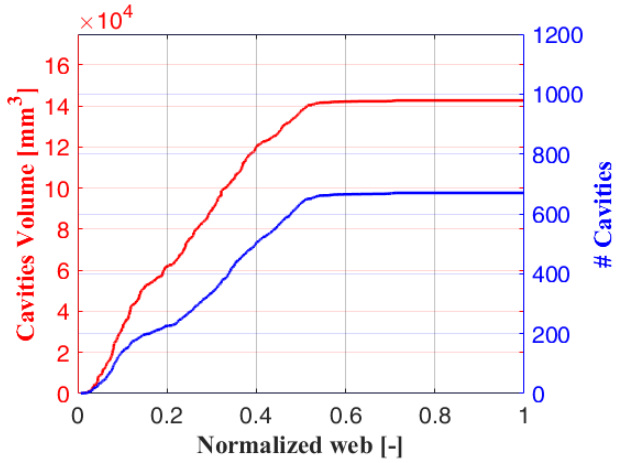

Fig. 16: Number and total volume of inclusions vs web coordinate

The effect of the detected inclusions can now be evaluated both in terms of performance modification (i.e., combustion surface changes), and in terms of longer exposure of the thermal protections of the motor case (i.e., web coordinate advance).

4.1 Effects on performance

The evaluation of the combustion surface change is performed by applying the methodology to each vertex of the mesh describing the burning surface at the different web coordinate values. Based on the considerations made in the validation phase of the procedure, the chosen edge size is $0.5\,mm$. The evaluated web advance has been used to represent the motion caused by the inclusions on each vertex, thus obtaining a geometrical representation of the modified surfaces, some of which are shown in Fig. 17. The regions affected by the inclusions are represented in a darker gray in order to better highlight them. As it can be noticed, even if the initial dimension of the inclusions is relatively small (see Fig. 17a), the extension of their effect spreads around due to the regression process (see Figures 17b and 17c).

Figures 17a-f show that all the inclusions generate effects within the portion of the motor that has been selected, thus confirming that the choice of taking into consideration only a portion of the original motor with the purpose of reducing the computational effort was right. Another aspect to be highlighted is the effect produced by adjacent surfaces characterized by different regression directions, such as the one that occurs in the lower part of the selected portion of the motor. Due to this, the initial circular shape of the inclusion located lowest in the drawings is progressively cut and modified by the advancement of the inclined burning surface connecting the cylindrical surfaces at the bottom and top of the motor.

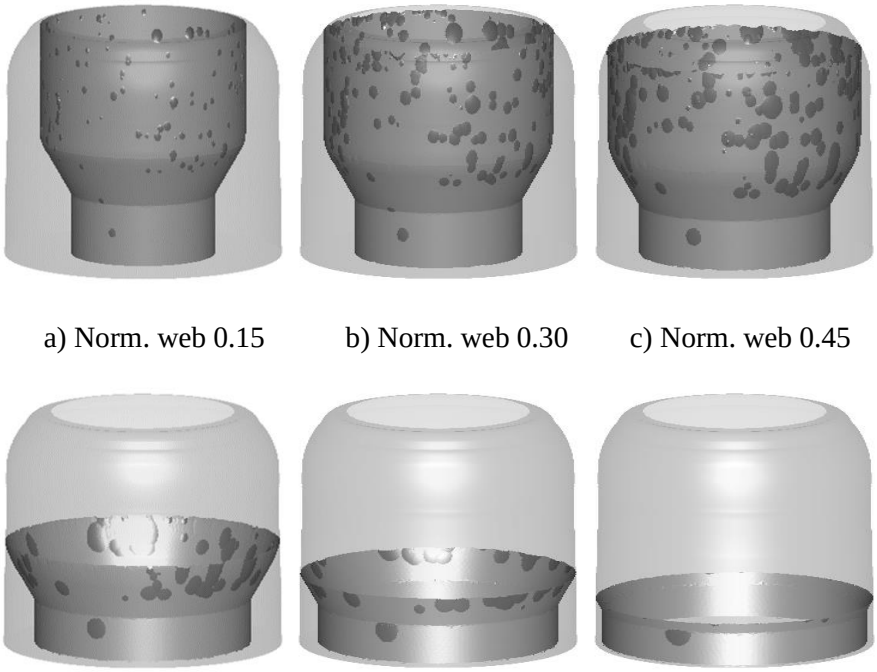

a) Norm. web 0.15 b) Norm. web 0.30 c) Norm. web 0.45

d) Norm. web 0.60 e) Norm. web 0.75 f) Norm. web 0.90

Fig. 17: Combustion surfaces at different web coordinates affected by the inclusions

The evaluation of the change of the regression area is reported in Fig. 18. The instantaneous absolute value can be as high as 7% of the maximum nominal combustion surface, even if the dimension of the inclusions is small. The maximum instantaneous absolute difference is located at approximately 55% of the web coordinate, in the region where the largest cylindrical portion of the motor's internal surface reaches the thermal protection layer. Such a large difference is due to the advance with which the thermal protection is hit, and to the corresponding reduction of the burning surface that disappears when the case is reached. It should be underlined that this large value is obtained because only a portion of the entire motor is represented. The value would have been lower than 1% (and, therefore, acceptable) if the total motor had been taken into consideration.

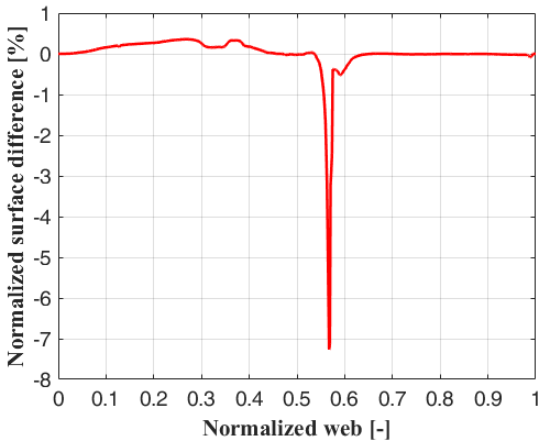

Fig. 18: Combustion surface percent variation vs web coordinate

During the first half of the propulsion phase, the combustion surface variation is positive, meaning that the amount of propellant burnt during that phase is larger than the nominal one. This is due to the propagation of the combustion surface, starting from the cavities, that increases the extension of the burning area and also the amount of propellant involved in the combustion process. In order to quantify this effect, the volume increase of burnt propellant with respect to the nominal condition is reported in Fig. 19.

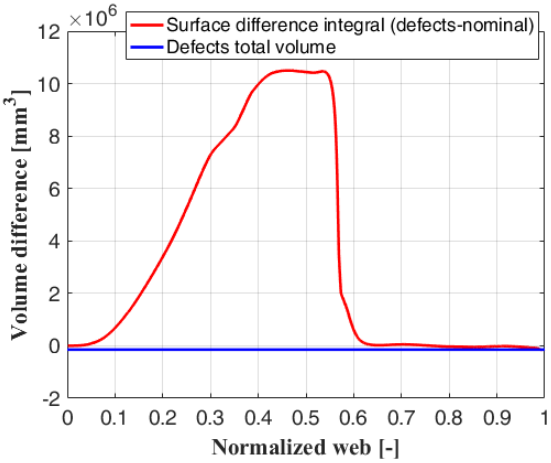

Fig. 19: Burned volume vs web coordinate

As can be observed in Fig. 19, the volume difference is quite high in the first half of the propellant's burning phase, with a peak in volume difference that is a lot higher than the total volume of the cavities. As already mentioned, this is due to the spreading of the burning surface of the cavities once they have been incorporated into the combustion process. At a normalized web equal to 0.55, this effect disappears since

most cavities are located in the upper region of the portion of the motor, characterized by a larger internal diameter and therefore a shorter burning time. The final value of the volume difference will be negative and equal to – in absolute value – the total volume of the cavities (reported in blue in Fig. 19), since the volume of the inclusions is filled with propellant in the nominal case, and empty in the real case.

4.2 Effects on the exposure time of thermal protections

The evaluation of the exposure time increase for the thermal protections is studied by applying the developed methodology to each vertex of the mesh describing the thermal protection surface. The smaller the mesh edge size, the higher the accuracy of the web advance obtained, as already discussed in previous sections. For this reason, the chosen mesh edge size is 0.5 *mm*. Fig. 20 shows the web advance value for the thermal protection surface, represented as a function of its curvilinear and angular coordinates (Fig. 20a) and reported on a 3D representation of the surface (Fig. 20b).

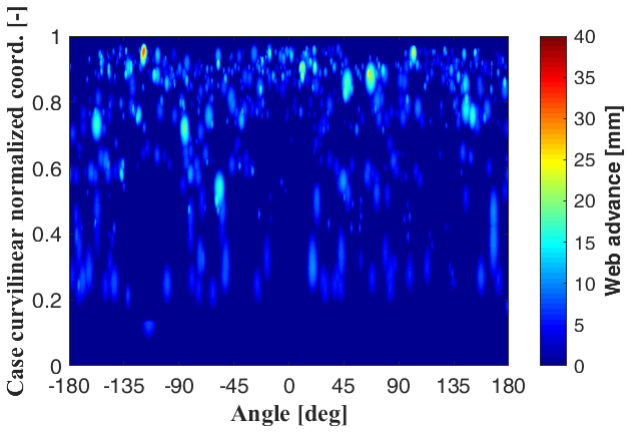

a) Web advance represented in curvilinear and angular coordinates

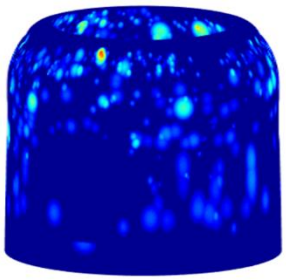

b) Web advance reported on the thermal protection surface

Fig. 20: Web advance obtained on the thermal protection surface

The same values are also reported on a waterfall representation in Fig. 21 in order to highlight the peak values, which appear to be as high as to 32 *mm*. Each web advance value obtained should be now checked to verify if the thermal protection is able to survive to the additional exposure to the high-temperature hot gases in the combustion chamber. Since the thickness of the thermal protection for this motor is a function of the curvilinear coordinate of the case only (i.e., the thickness does not vary in the angular direction), the piece of information that is needed to complete this check is the maximum web advance for each value of the curvilinear coordinate, as reported in Fig. 22.

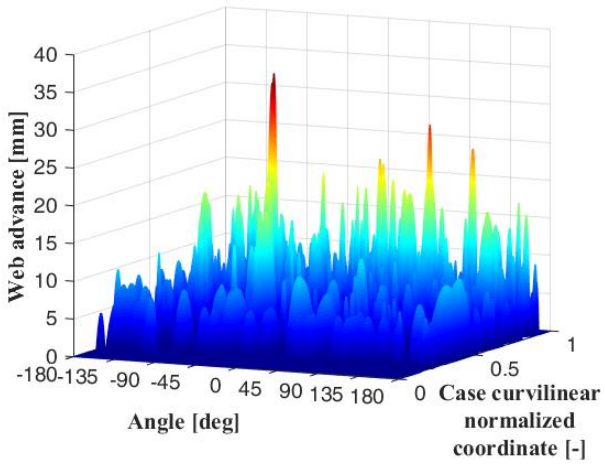

Fig. 21: Waterfall representation of the web advance

The values reported in Fig. 22 have been obtained by simply considering the maximum web advance estimated for each case curvilinear coordinate. Since the maximum diameter of the detected cavities is equal to 14 *mm* approximately, and the maximum web advance is more than twice that value, there is a strong effect of mutual influence between inclusions. In particular, the highest value is the effect of the combination of 5 cavities (with a maximum nominal diameter of 11.5 *mm*) which are almost aligned on the line that describes the path followed by combustion to reach the corresponding position on the thermal protection.

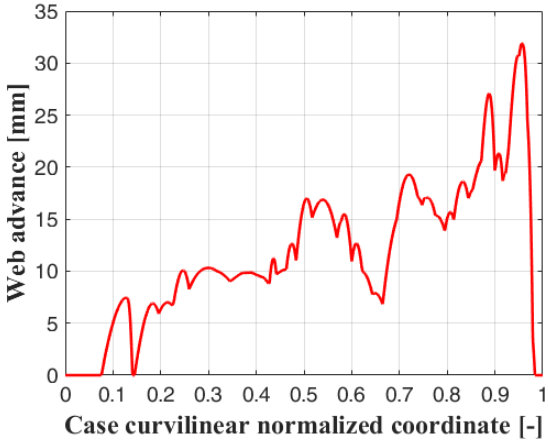

Fig. 22: Maximum value of web advance as a function of case curvilinear coordinate

4.3 Effect of uncertainties

The final point to be evaluated in the present study was the effect of the uncertainties on the properties of the cavities. The assumption is that the maximum uncertainty on the diameter of each cavity is 1 mm, whereas the knowledge of the position is less accurate, and the inaccuracy can be as high as 10 mm. This larger inaccuracy stems from the fact that the position of each cavity is obtained by matching together different views of the same cavity, obtained through X-ray investigations of the same grain portion seen from different view angles.

The methodology described in the previous section has been employed to determine the worst condition for each point on the thermal protection surface. As already mentioned in the methodology description, each thermal protection surface point has its own worst condition, determined by a dedicated application of the inaccuracies (especially in terms of position). For this reason, the worst global condition is the collection of all the worst results determined for each position on the investigated surface and obtained with different cavity configurations. The worst global condition represents a collection of web advances that can be obtained locally but cannot be obtained with the same intensity starting from a single cavity configuration. The comparison between the maximum web advance for each value of the curvilinear coordinate under the nominal cavity configuration and the one resulting from taking into consideration the collection of the worst cases is shown in Fig. 23.

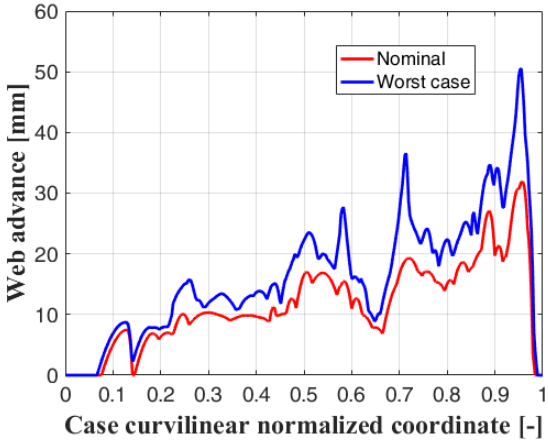

Fig. 23: Comparison between nominal inclusion configuration and worst case

The total number of simulations performed to determine the worst condition for each point of the thermal protection surface was equal to 275 000 and required approximately 70 hours of work to be completed.

The highest value of the web advance is still in the same position, even if its value is higher by 20 *mm*, amounting to a 60% increase. That increase cannot be explained simply by considering the diameter growth introduced with the uncertainties, since the 5 cavities involved in the nominal configuration to generate the maximum web advance level would have generated a 5 mm increase maximum. This means that other cavities exert an influence for that position once they have been considered in their most dangerous position: as a matter of fact, the total number of cavities playing a role rises to 9.

The difference obtained between nominal cavity configuration and worst-case application of the inaccuracies highlights the importance of considering this effect. The increment of the highest web advance is indeed substantial, and its exact evaluation is crucial in guaranteeing the safety of the motor under study.

5 Conclusions

A methodology to evaluate the effects of cavities inside the grain of a solid rocket motor has been developed and validated. The methodology has been presented in detail by taking into account inclusions with a spherical shape, however, it may be extended to cavities with a generic shape by simply considering them as being composed of a set of spherical inclusions. The output of the developed procedure is the change in burning surface (linked to the change in internal pressure and generated thrust), and the variation of exposure time of the thermal protection surface. This set of information is needed each time a set of inclusions is detected inside a manufactured rocket to make sure that the motor can be safely launched. In the validation phase, the methodology was proven effective as long as the dimensions of the edge size of

the mesh employed to describe the burning surface and/or the thermal protection surface is small enough. Under these conditions, it is indeed possible to guarantee an accuracy that remains under 1% of the variations generated by the presence of the cavities.

The procedure has been extended to assess the effects generated by the inaccuracies in the measuring of the dimension and position of the cavities – usually detected through X-ray inspection of the grain. The outcome of the methodology is in the collection of the local worst-case scenarios, obtained as the result of the combination of the most dangerous positioning and sizing of the inclusions within the inaccuracy limits. The algorithm has been applied to an actual motor containing a large number of inclusions (670), produced during the manufacturing process. The methodology was proven effective in the evaluation of the consequences caused by the presence of the cavities, highlighting their mutual interactions that would not have been otherwise considered. The highest exposure advance of the thermal protection surface was located in a region in which 5 different inclusions were interacting, generating an advance approximately 3 times higher than the maximum diameter of the largest cavity of the cluster. The methodology can be applied to any motor simply by knowing its geometry and dimension and location of its cavities.

Nomenclature

D_{cav} = diameter of the cavity [m]

$dist_{12}$ = distance between the centers of cavity 1 and cavity 2 [m]

$dist_{p1}$ = distance between point P and the center of cavity 1 [m]

$dist_{p2}$ = distance between point P and the center of cavity 2 [m]

$dist_{pcav}$ = distance between the center of the cavity and the generic point P [m]

w = web coordinate [m]

w_{cav} = web coordinate in which the cavity is incorporated into the burning surface [m]

$w_{cav2cav1}$ = web coordinate in which cavity 2 is reached by the combustion coming from cavity 1 [m]

w_{cen} = web coordinate of the cavity center [m]

w_p = web coordinate on a generic point P [m]

w_{pcav} = web coordinate in which point P is reached by the combustion coming from the cavity [m]

x = coordinate of points along x-axis [m]

y = coordinate of points along y-axis [m]

z = coordinate of points along z-axis [m]

Δw_{21} = web advance caused by cavity 1 on cavity 2 [m]

Δw_i = web advance on the i-th cavity caused by a set of cavities [m]

Δw_p = web advance on point P caused by a set of cavities [m]

Δw_{p1} = web advance caused by cavity 1 on point P [m]

Δw_{p2} = web advance caused by cavity 2 on point P [m]

Δw_{pcav} = web advance caused by a cavity on point P [m]

Declaration of competing interest

The authors declare that they have no known competing financial interests or personal relationships that could have appeared to influence the work reported in this paper.

References

[1] A. Davenas, J. Thépenier, Recent progress in the prediction and analysis of the operation of solid rocket motors, Acta Astronaut. 44 (1999) 461–469. https://doi.org/10.1016/S0094-5765(99)00079-X.

[2] D. Dhital, J.R. Lee, C. Farrar, D. Mascarenas, A review of flaws and damage in space launch vehicles: Motors and engines, J. Intell. Mater. Syst. Struct. 25 (2014) 524–540. https://doi.org/10.1177/1045389X13493360.

[3] R. Taherinezhad, G. Zarepour, S.S. Tabatabayee, Evaluation of Failure Factors of a Small-Scale Motor in Laboratory Testing, J. Fail. Anal. Prev. 20 (2020) 617–626. https://doi.org/10.1007/s11668-020-00878-x.

[4] P. Le Breton, D. Ribereau, Casting Process Impact on Small-Scale Solid Rocket Motor Ballistic Performance, J. Propuls. Power. 18 (2002) 1211–1217. https://doi.org/10.2514/2.6055.

[5] G. Sutton, O. Biblarz, Rocket Propulsion Elements 9th Edition, Rocket Propuls. Elem. (2016).

[6] S. BEAN, Predicting X-rays for dynamic flaw detection in solid rockets, in: 27th Jt. Propuls. Conf., American Institute of Aeronautics and Astronautics, Reston, Virigina, 1991. https://doi.org/10.2514/6.1991-3367.

[7] P. Lamarque, SRM improved X-rays examination: automatic detection in sight, Acta Astronaut. 54 (2004) 487–492. https://doi.org/10.1016/S0094-5765(03)00206-6.

[8] B. Ghose, D.K. Kankane, Estimation of location of defects in propellant grain by X-ray radiography, NDT E Int. 41 (2008) 125–128. https://doi.org/10.1016/j.ndteint.2007.08.005.

[9] H. Esiyok, M.E. Candarli, THEORETICAL AND EXPERIMENTAL PACKING DENSITY STUDY OF HYDROXYL TERMINATED POLYBUTADIENE-AMMONIUM PERCHLORATE BASED PROPELLANT AND ITS INFLUENCE ON BURNING RATE, Int. J. Energ. Mater. Chem. Propuls. 13 (2014) 455–469. https://doi.org/10.1615/IntJEnergeticMaterialsChemProp.2014011241.

[10] M. Kohga, Effect of Voids inside AP Particles on Burning Rate of AP/HTPB Composite Propellant, Propellants, Explos. Pyrotech. 33 (2008) 249–254. https://doi.org/10.1002/prep.200700234.

[11] F. Gibou, R. Fedkiw, S. Osher, A review of level-set methods and some recent applications, J. Comput. Phys. 353 (2018) 82–109. https://doi.org/10.1016/j.jcp.2017.10.006.

[12] M.A. Willcox, M.Q. Brewster, K.C. Tang, D.S. Stewart, Solid Propellant Grain Design and Burnback Simulation Using a Minimum Distance Function, J. Propuls. Power. 23 (2007) 465–475. https://doi.org/10.2514/1.22937.

[13] Y.-H. Hwang, C.-H. Chiang, Simple Surface-Tracking Methods for Grain Burnback Analysis, J. Propuls. Power. 31 (2015) 1436–1444. https://doi.org/10.2514/1.B35682.

[14] M.A. Willcox, M.Q. Brewster, K.C. Tang, D.S. Stewart, I. Kuznetsov, Solid Rocket Motor Internal Ballistics Simulation Using Three-Dimensional Grain Burnback, J. Propuls. Power. 23 (2007) 575–584. https://doi.org/10.2514/1.22971.

[15] M. Plaud, S. Gallier, M. Morel, Simulations of heterogeneous propellant combustion : Effect of particle orientation and shape, Proc. Combust. Inst. 35 (2015) 2447–2454. https://doi.org/10.1016/j.proci.2014.05.020.

[16] V.N. Emelyanov, I.V. Teterina, K.N. Volkov, Dynamics and combustion of single aluminium agglomerate in solid propellant environment, Acta Astronaut. 176 (2020) 682–694. https://doi.org/10.1016/j.actaastro.2020.03.046.

[17] O. Orlandi, M. Plaud, F. Godfroy, S. Larrieu, N. Cesco, Aluminium droplets combustion and SRM instabilities, Acta Astronaut. 158 (2019) 470–479. https://doi.org/10.1016/j.actaastro.2019.03.036.

[18] L. Massa, T.L. Jackson, M. Short, Numerical solution of three-dimensional heterogeneous solid propellants, Combust. Theory Model. 7 (2003) 579–602. https://doi.org/10.1088/1364-7830/7/3/308.

[19] X. Wang, T.L. Jackson, L. Massa, Numerical simulation of heterogeneous propellant combustion by a level set method, Combust. Theory Model. 8 (2004) 227–254. https://doi.org/10.1088/1364-7830/8/2/003.

[20] X. Wang, T. Jackson, The numerical simulation of two-dimensional aluminized composite solid propellent combustion, Combust. Theory Model. 9 (2005) 171–197. https://doi.org/10.1080/13647830500098415.

[21] X. Wang, T.L. Jackson, J. Buckmaster, Numerical simulation of the 3-dimensional combustion of aluminized heterogeneous propellants, Proc. Combust. Inst. 31 (2007) 2055–2062. https://doi.org/10.1016/j.proci.2006.07.136.

[22] D. Ribereau, P. Le Breton, S. Ballereau, Casting process effect on composite solid propellant burning rate, in: 37th Jt. Propuls. Conf. Exhib., American Institute of Aeronautics and Astronautics, Reston, Virigina, 2001. https://doi.org/10.2514/6.2001-3946.

[23] P. Le Breton, D. Ribereau, C. Marraud, P. Lamarque, EXPERIMENTAL AND NUMERICAL STUDY OF CASTING PROCESS EFFECTS ON SMALL SCALE SOLID ROCKET MOTOR BALLISTIC BEHAVIOR, Int. J. Energ. Mater. Chem. Propuls. 5 (2002) 132–145. https://doi.org/10.1615/IntJEnergeticMaterialsChemProp.v5.i1-6.160.

[24] T.L. Jackson, Modeling of Heterogeneous Propellant Combustion: A Survey, AIAA J. 50 (2012) 993–1006.

https://doi.org/10.2514/1.J051585.

[25] G.M. Knott, T.L. Jackson, J. Buckmaster, Random Packing of Heterogeneous Propellants, AIAA J. 39 (2001) 678–686. https://doi.org/10.2514/2.1361.

[26] S. Kochevets, J. Buckmaster, T.L. Jackson, A. Hegab, Random Packs and Their Use in Modeling Heterogeneous Solid Propellant Combustion, J. Propuls. Power. 17 (2001) 883–891. https://doi.org/10.2514/2.5820.

[27] R. MILLER, Effects of particle size on reduced smoke propellant ballistics, in: 18th Jt. Propuls. Conf., American Institute of Aeronautics and Astronautics, Reston, Virigina, 1982. https://doi.org/10.2514/6.1982-1096.

[28] D. Ribereau, F. Dauch, G. Fouin, R. Lefrere, Assessment of solid propellant motor internal ballistics at full-scale with ultrasound measurements, in: 36th AIAA/ASME/SAE/ASEE Jt. Propuls. Conf. Exhib., American Institute of Aeronautics and Astronautics, Reston, Virigina, 2000. https://doi.org/10.2514/6.2000-3844.

[29] T.L. Jackson, J. Buckmaster, J. Hoeflinger, Three-dimensional flames supported by heterogeneous propellants, Proc. Combust. Inst. 28 (2000) 895–902. https://doi.org/10.1016/S0082-0784(00)80295-7.

[30] M.L. Gross, M.W. Beckstead, Steady-State Combustion Mechanisms of Ammonium Perchlorate Composite Propellants, J. Propuls. Power. 27 (2011) 1064–1078. https://doi.org/10.2514/1.B34053.

[31] W. Ao, X. Liu, H. Rezaiguia, H. Liu, Z. Wang, P. Liu, Aluminum agglomeration involving the second mergence of agglomerates on the solid propellants burning surface: Experiments and modeling, Acta Astronaut. 136 (2017) 219–229. https://doi.org/10.1016/j.actaastro.2017.03.013.

[32] F. Dauch, D. Ribereau, A Software for SRM Grain Design and Internal Ballistics Evaluation, PIBAL, in: 38th AIAA/ASME/SAE/ASEE Jt. Propuls. Conf. & Exhib., American Institute of Aeronautics and Astronautics, Reston, Virigina, 2002. https://doi.org/10.2514/6.2002-4299.

[33] X. Wang, K. Hossain, T.L. Jackson, The three-dimensional numerical simulation of aluminized composite solid propellant combustion, Combust. Theory Model. 12 (2008) 45–71. https://doi.org/10.1080/13647830701395099.

[34] L. Massa, T.L. Jackson, J. Buckmaster, Using Hetergeneous Propellant Burning Simulations as Subgrid Components of Rocket Simulations, AIAA J. 42 (2004) 1889–1900. https://doi.org/10.2514/1.4445.

[35] J. Szmelter, P. Ortiz, Burning surfaces evolution in solid propellants: A numerical model, Proc. Inst. Mech. Eng. Part G J. Aerosp. Eng. 221 (2007) 429–439. https://doi.org/10.1243/09544100JAERO102.

[36] D. Ribereau, P. Le Breton, E. Giraud, SRM 3D surface burnback computation using mixes stratification deduced from 3D grain filling simulation, in: 35th Jt. Propuls. Conf. Exhib., American Institute of Aeronautics and Astronautics, Reston, Virigina, 1999. https://doi.org/10.2514/6.1999-2802.

[37] P. REN, H. WANG, G. ZHOU, J. LI, Q. CAI, J. YU, Y. YUAN, Solid rocket motor propellant grain burnback simulation based on fast minimum distance function calculation and improved marching tetrahedron method, Chinese J. Aeronaut.

34 (2021) 208–224. https://doi.org/10.1016/j.cja.2020.08.052.

[38] R. Bertacin, F. Ponti, E. Corti, D. Fedele, A. Annovazzi, Numerical Simulation of the Zefiro 9 Performance Using a New Dynamic SRM Ballistic Simulator, in: 49th AIAA/ASME/SAE/ASEE Jt. Propuls. Conf., American Institute of Aeronautics and Astronautics, Reston, Virginia, 2013. https://doi.org/10.2514/6.2013-4174.

[39] P. Le Breton, D. Ribereau, F. Godfroy, R. Abgrall, S. Augoula, SRM performance analysis by coupling bidimensional surface burnback and pressure field computations, in: 34th AIAA/ASME/SAE/ASEE Jt. Propuls. Conf. Exhib., American Institute of Aeronautics and Astronautics, Reston, Virigina, 1998. https://doi.org/10.2514/6.1998-3968.

[40] R. Bertacin, F. Ponti, A. Annovazzi, A New Three-Dimensional Ballistic Model for Solid Rocket Motor Non-Homogeneous Combustion, in: 48th AIAA/ASME/SAE/ASEE Jt. Propuls. Conf. & Exhib., American Institute of Aeronautics and Astronautics, Reston, Virigina, 2012. https://doi.org/10.2514/6.2012-3974.

[41] F. Ponti, S. Mini, A. Annovazzi, Numerical Evaluation of the Effects of Inclusions on Solid Rocket Motor Performance, AIAA J. 58 (2020) 4028–4036. https://doi.org/10.2514/1.J058735.

[42] D. Gamdha, S. Unnikrishnakurup, K.J.J. Rose, M. Surekha, P. Purushothaman, B. Ghose, K. Balasubramaniam, Automated Defect Recognition on X-ray Radiographs of Solid Propellant Using Deep Learning Based on Convolutional Neural Networks, J. Nondestruct. Eval. 40 (2021) 18. https://doi.org/10.1007/s10921-021-00750-4.

[43] F. Ponti, S. Mini, A. Annovazzi, A simplified approach to predict Friedman Curl effect in a solid rocket motor using ROBOOST simulation tool, in: AIAA Propuls. Energy 2019 Forum, American Institute of Aeronautics and Astronautics, Reston, Virginia, 2019. https://doi.org/10.2514/6.2019-3960.

Vitae

Fabrizio Ponti, received his PhD in Machine Engineering from Polytechnic of Bari, Italy, in 2001. He is currently Full Professor at University of Bologna since 2018, teaching Aerospace Propulsion within the Master in Aerospace Engineering. His main research interests are Solid Rocket Boosters simulation and modeling with particular focus on 3D modeling of the burnback process, thermal protection ablation, internal ballistics, and flaws modeling. He is also involved in other research topics dealing with the modeling of the combustion process in internal combustion engines and gas turbines.

Stefano Mini, PhD in Mechanics and Advanced Engineering Scineces.

Research Fellow at the University of Bologna, Department of Industrial Engineering. He received his master's degree in Aerospace Engineering with a thesis regarding the design and implementation of a self-intersection removal procedure for a solid rocket motor simulation program.

His research interest revolves around the modelling and design of simulators with the aim of giving predictions about solid rocket motor performances. He is currently working on the modelling of the thermal protection materials ablation phenomenon and their effect on the thrust final phase.

Luca Fadigati received his bachelor's and master's degree in Aerospace Engineering at University of Bologna, Forlì, Italy in 2016, and in 2020 respectively. He is currently enrolled in a PhD course in Mechanics and Advanced Engineering Science at the Faculty of Aerospace Engineering, University of Bologna. His research interests center on solid rocket propulsion, focusing on the simulation of case insulating thermal protection material ablation.

Vittorio Ravaglioli, PhD in Mechanics and Advanced Engineering Sciences.

Senior Assistant Professor at the University of Bologna, Department of Industrial Engineering.

Academic Lecturer for the courses of Turbomachines (bachelor's in Aerospace Engineering) and Internal Combustion Engines (International Master in Advanced Automotive Engineering).

Personal research activities mainly focused on the development of models and innovative control strategies for Advanced Propulsion Systems, both in Aerospace and Automotive field.

Adriano Annovazzi, Senior Engineer at AVIO Space Propulsion Design Department. He was responsible for grain design and motor performance of military rocket missiles and Ariane 4/Ariane 5 solid boosters. Moreover, he focused on hybrid rocket motor design. Regarding the above-mentioned activities, he was involved as co-author in articles published in international journals.

At present, his activity revolves around numerical codes to give predictions concerning solid motor internal ballistics.

Valentina Garreffa, she received her master's degree in Aerospace Engineering at University of La Sapienza, Roma, Italy in 2009. She is currently Senior Engineer at AVIO Space Propulsion Design Department since 2010. She is responsible of definition and motor performance of Avio first stage solid rockets: MPS, P80, P120 and Z40FS for Vega and Ariane5 launchers.